Shell-model calculations of Gamow-Teller strength in ^{51}V, ^{54}Fe, and ^{59}Co

Maurice B. Aufderheide, Stewart D. Bloom, David A. Resler, and Grant J. Mathews
Physics Department, Lawrence Livermore National Laboratory, Livermore, California 94550
(Received 13 May 1993)

The Gamow-Teller (GT) strength functions of ^{51}V, ^{54}Fe, and ^{59}Co measured by recent charge-exchange experiments have been studied using shell-model calculations employing two model spaces. The shell model is fairly successful at reproducing GT strength in the (p,n) direction, but the agreement is not as good in the (n,p) direction. It is found that both directions can be fit consistently by shifting single particle energies in a systematic manner. It is found that roughly 75% of the sum-rule strength can be seen in the experiments for both ^{51}V and ^{54}Fe. It is also found that roughly 35% of the GT strength predicted by the shell model is seen in the (n,p) direction for all three nuclei, but that the quenching in the (p,n) direction varies with nucleus. The consequences of these findings for improving the calculation of weak interaction rates are discussed.

PACS number(s): 23.40.−s, 25.40.Ep, 25.40.Fq, 21.60.Cs

I. INTRODUCTION

Because of energetics, terrestrial electron capture and $\beta^{\pm}$ decay reactions do not generally sample the allowed Gamow-Teller (GT) and Fermi strength functions over a very large range of daughter excitation energy. In the last decade however, charge-exchange reactions, such as (p,n) and (n,p) at incident energies greater than 100 MeV have been used to probe these strength functions over a much larger energy range. At such energies, the measured charge-exchange cross section at 0° is roughly proportional to the Fermi and Gamow-Teller matrix elements from the parent ground state to states in the daughter [1,2]. The results of García *et al.* [3] in the $A=37$ system have lead Adelberger, García, and Wells [4] to question the validity of this statement, but there remain questions regarding the interpretation of the García *et al.* experiment [5,6]. Here we adopt the viewpoint that future work will vindicate charge-exchange reactions as reliable probes of GT and Fermi strength.

The (p,n) reaction measures GT strength in the "isospin-lowering" direction, and thus measures the β^- decay strength function, S_-. This reaction also excites the isobaric analog state (IAS) of the parent in the daughter nucleus, which contains the Fermi strength for the transition. The presence of this strong Fermi transition in the midst of S_- makes the extraction of GT strength more difficult because the two types of strength are proportional to the cross section with different energy-dependent factors of proportionality. In (p,n) reactions on the fp shell nuclei, S_- typically exhibits a strong resonant peak 10–15 MeV above the daughter ground state, the GT giant resonance.

The (n,p) reaction measures GT strength in the "isospin-raising" direction, thus measuring the electron-capture strength function, S_+. No IAS is seen in this reaction because of isospin considerations. These reactions typically exhibit a resonant peak 1–10 MeV above the daughter ground state for the fp nuclei of concern here.

In late stages of the evolution of type II supernova progenitors, fp shell nuclei become abundant in the core of the star as the ashes of silicon burning. Because of the high density of this "iron core," the electrons, which provide most of the core's support pressure, become highly degenerate. The large Fermi energy of the electrons allows a sizeable fraction of the electrons to reach the GT resonance strength. As a result, the electron capture rates of these nuclei can be dramatically enhanced. Bethe *et al.* [7] first recognized this effect and Fuller, Fowler, and Newman [8–11] were the first to compute rates for large numbers of fp shell nuclei using the independent single-particle shell model [12]. They did not, however, use full shell-model calculations to estimate the location of GT resonances. Phase-space considerations make these rates extremely sensitive to where the GT resonances lie in the daughter nuclei. Recent work [13] has indicated that the locations of these resonances need to be computed accurately, in order to obtain reliable rates.

Full shell-model calculations of S_- and S_+ would be extremely useful for fp shell nuclei of astrophysical interest. If they are to be trustworthy for such work, the calculations should faithfully reproduce the strength functions which have been measured. That is, the general shape and location of the strength function should be accurately described. Furthermore, it is well known that the total measured GT strength is much less than what is predicted by shell-model calculations. Such quenching [14,15] of the shell-model strength must be incorporated by fiat (see Secs. II and III), lacking a conclusive demonstration of its causes. Comparison with experimental strength functions provides guidance for nuclei which have not been (or cannot be) measured.

In this paper we consider ^{51}V, ^{54}Fe, and ^{59}Co, the three fp shell nuclei with $50<A<60$ for which S_+ has been measured. We calculate GT strength functions for these nuclei using a full shell model. Our goal is to explore how reliably we can generate the nuclear physics information needed for stellar electron-capture rates. In the second section, we summarize and discuss the most recent exper-

imental results for these nuclei. In the third section, a two-body interaction is used to calculate S_+ and S_- and the effect of shifts of single-particle energies are investigated. In the last part of this paper, we discuss how well the experimental results are reproduced and how these results affect astrophysical studies.

II. EXPERIMENTAL DATA

Figure 1 shows the (p,n) cross sections for ^{51}V and ^{54}Fe as measured by Rapaport *et al.* [16] and Anderson *et al.* [17], respectively [to our knowledge, ^{59}Co has not been used as a target for (p,n) reactions]. The IAS can be seen at 6.61 and 0 MeV for ^{51}V and ^{54}Fe, respectively. The giant GT resonance can be seen near 12.5 and 9.5 MeV for ^{51}V and ^{54}Fe, respectively. For ^{54}Fe, the giant GT resonance has been resolved into three components due to improved experimental resolution. Both strength functions exhibit giant resonances with some amount of GT strength at intermediate excitation energies (4–7 MeV) in the daughter. The strength seen in ^{51}V is generally several MeV above similar structures in ^{54}Fe.

Figure 2 shows the GT strength extracted from (n,p) experiments on ^{51}V, ^{54}Fe, and ^{59}Co. The ^{54}Fe results are from Vetterli *et al.* [18]. The ^{51}V and ^{59}Co results are from TRIUMF experiment E629 [19], which recently measured (n,p) reactions on these nuclei with 200 MeV incident neutrons. The GT resonances from ^{51}V, ^{54}Fe, and ^{59}Co are at 5, 1, and 4 MeV, respectively. It is interesting that, while both S_+ and S_- for ^{51}V show GT strength at higher daughter excitation energies than for ^{54}Fe, the amount of strength seen in S_+ is much less for ^{51}V than for ^{54}Fe.

Table I lists the total GT strength measured by each charge-exchange experiment. The total strength in both directions for a particular nucleus,

$$B(\mathrm{GT})_{\pm}=\int S_{\pm}dE \ ,$$

obeys the theoretical sum rule [14]

$$B(\mathrm{GT})_{-}-B(\mathrm{GT})_{+}=3(N-Z) \ , \qquad (1)$$

where N is the number of neutrons and Z is the number of protons in the parent nucleus. There is more strength in the (p,n) direction for ^{51}V than ^{54}Fe because there are fewer protons blocking conversion of neutrons into protons in the former nucleus. Conversely, the larger number

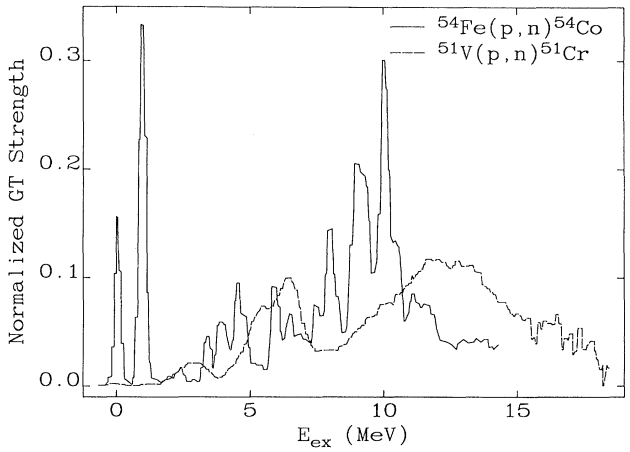

FIG. 1. Measured (p,n) cross sections for ^{51}V [16] and ^{54}Fe [17]. There has not been a corresponding measurement for ^{59}Co. The GT strength functions are directly proportional to these cross sections, except for the region of the IAS, where Fermi strength is also present. The IAS lies at 6.61 and 0 MeV for ^{51}V and ^{54}Fe, respectively.

of protons in ^{54}Fe makes the strength in the (n,p) direction larger for ^{54}Fe than ^{51}V. One would expect $B(\mathrm{GT})_+$ to be even larger for ^{59}Co, since it has one more proton than ^{54}Fe, but this is not seen experimentally. The four extra neutrons above the filled $1f_{7/2}$ orbital in ^{59}Co tend to block the GT strength in the (n,p) direction, thus weakening the GT strength in this nucleus. If $B(\mathrm{GT})_-$ were measured for ^{59}Co, we would expect it to be larger than the strength seen in ^{54}Fe and probably ^{51}V, because there are four more neutrons which can contribute to the GT strength in the (p,n) direction.

As can be seen by comparing the fourth and fifth columns of Table I, the sum rule is clearly quenched. By "quenching" we mean that less GT strength has been directly measured by the experiments than is predicted by the sum rule. The missing strength presumably resides at higher energies than can presently be reached by charge-exchange experiments. This strength is referred to as "missing" because $0\hbar\omega$ shell-model calculations predict that the total GT strength should be seen at energies accessible to charge-exchange experiments. This is the sense in which we say that the GT strength is "missing" and thus "quenched." Goodman, Rapaport, and Bloom

TABLE I. Measurements of GT strength in ^{51}V, ^{54}Fe, and ^{59}Co compared with theoretical sum rule. The "Total strength" columns list measured strength in sum rule units. The "Sum rule" columns compare the measured sum rule with the theoretical prediction. The last column lists what fraction of the total sum rule was seen in each experiment. Because ^{50}Co$(p,n)^{59}$Ni has never been measured, it is not possible to test its sum rule.

	Total strength		Sum rule		
Nucleus	(p,n)	(n,p)	Exp.	Theor.	Q_{SR}
^{51}V	12.6±2.50	1.48±0.03	11.12±2.50	15	0.74±0.17
^{54}Fe	7.5±0.7	3.09±0.57	4.41±0.90	6	0.74±0.15
^{59}Co		2.39±0.07		15	

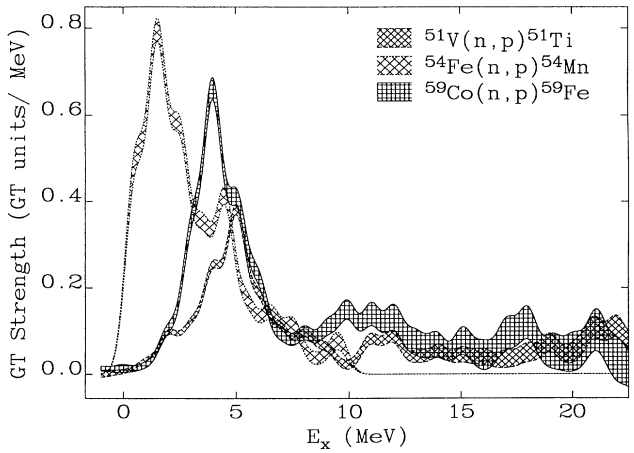

FIG. 2. GT strength functions as measured by (n,p) reactions on ^{51}V [19], ^{54}Fe [18], and ^{59}Co [19]. The crosshatched regions in each case show the experimental uncertainties.

[20] have emphasized that such comparisons are strictly a test of the completeness of experimental measurements of the strength functions, and not a test of the sum rule itself. The quenching of the sum rule, $\mathcal{Q}_{\rm SR}$, is estimated in the last column of Table I where

$$\mathcal{Q}_{\rm SR}=\frac{[B({\rm GT})_- - B({\rm GT})_+]_{\rm Expt.}}{[B({\rm GT})_- - B({\rm GT})_+]_{\rm Theory}} . \quad (2)$$

The values of $\mathcal{Q}_{\rm SR}$ for ^{51}V and ^{54}Fe are in good agreement. It appears that this amount of quenching (i.e., this incompleteness of experimental measurements of the strength functions) may be a common feature of fp shell nuclei.

If we assume that the $\mathcal{Q}_{\rm SR}$ is a constant for nuclei in this mass range, we can estimate $B({\rm GT})_-$ for ^{59}C. Using the value of $\mathcal{Q}_{\rm SR}$ for ^{51}V and ^{54}Fe, the sum-rule strength for ^{59}Co would be 11.12. This would imply $B({\rm GT})_- \sim 13.5$, which is somewhat larger than the value seen in ^{51}V. Such a result would be consistent with the trends in strength discussed above. No uncertainties have been estimated because it is not clear how accurate the assumption of a constant amount of sum-rule quenching is. A measurement of ^{59}Co$(p,n)^{59}$Ni would help to answer this question, because ^{59}Co is quite different from ^{51}V and ^{54}Fe.

III. SHELL-MODEL RESULTS

Shell-model calculations in the mass range of interest here, $50 \le A \le 60$, are difficult because the number of nucleons in the fp shell is large enough that full $0\hbar\omega$ calculations are presently not possible. A truncated model space must therefore be chosen which is small enough that calculations are tractable, but large enough that important physics (such as satisfying the GT sum rule) is present in the model. Because of these difficulties, there are not many interactions which have been developed for this mass range.

In this paper, we use the FPVH interaction [21,22]. This interaction uses the interaction of van Hees and Glaudemans [21] for the eight matrix elements which only connect the $1f_{7/2}$ orbital to itself and uses the van Hienen, Chung, and Wildenthal interaction [22] for the rest of the matrix elements. Both pieces are effective Hamiltonians which were obtained by fits to a large number of measured nuclear properties such as binding energies, low-energy spectra, $M1$ and $E2$ moments, and log ft values. The FPVH interaction was designed for the study of isotopes with $A \sim 54$ and for Ni, Cu, and Zn isotopes. The model space is clearly defined by FPVH. For the low-mass range, the model space is

$$(1f_{7/2})^n + (1f_{7/2})^{n-1}(2p_{3/2}2p_{1/2}1f_{5/2})^1 ,$$

where n is the number of nucleons in the fp shell. In the upper mass range, the model space is

$$(1f_{7/2})^{16}(2p_{3/2}2p_{1/2}1f_{5/2})^k ,$$

where $n = 16+k$ and the ^{56}Ni core is closed. Only the k nucleons above this core are free to move. For ^{51}V, the model space is

$$(1f_{7/2})^{11} + (1f_{7/2})^{10}(2p_{3/2}2p_{1/2}1f_{5/2})^1 ,$$

while for ^{54}Fe the model space is

$$(1f_{7/2})^{14} + (1f_{7/2})^{13}(2p_{3/2}2p_{1/2}1f_{5/2})^1 .$$

^{59}Co is an intermediate case because it has neutrons above the $1f_{7/2}$ oribtal, but the proton $1f_{5/2}$ orbital is not filled. The model space could be either

$$(1f_{7/2})^{15}(2p_{3/2}2p_{1/2}1f_{5/2})^4$$

or

$$(1f_{7/2})^{15}(2p_{3/2}2p_{1/2}1f_{5/2})^4 + (1f_{7/2})^{14}(2p_{3/2}2p_{1/2}1f_{5/3})^5 .$$

The dimension for each of these parent spaces is given in Table II.

Because the model spaces considered here are limited, it is necessary to ensure that the sum rule is satisfied. The sum rule is satisfied if an extra nucleon in the $1f_{7/2}$ orbital of the daughter nucleus is allowed to be excited to the other fp orbitals in addition to the excitations allowed in the parent model space. Thus, the daughter model spaces are, in general, much larger than the parent spaces and usually determine whether a calculation of the GT strength function is feasible. It can be seen in Table II that calculations in the (p,n) direction typically involve much larger daughter model spaces than the (n,p) direction. In fact, the large model space for ^{59}Co$(p,n)^{59}$Ni is too large to be computed with presently available resources and only the small model space is calculated for this channel.

The CRUNCHER shell-model code [23] was used in these calculations. For each of the strength function calculations, 10 Lanczos iterations were performed for each allowed daughter J^π value, and the resulting widths of the 27 (or 9 for ^{54}Fe) quasieigenstates were used in plotting the strength functions. The theoretical width of each

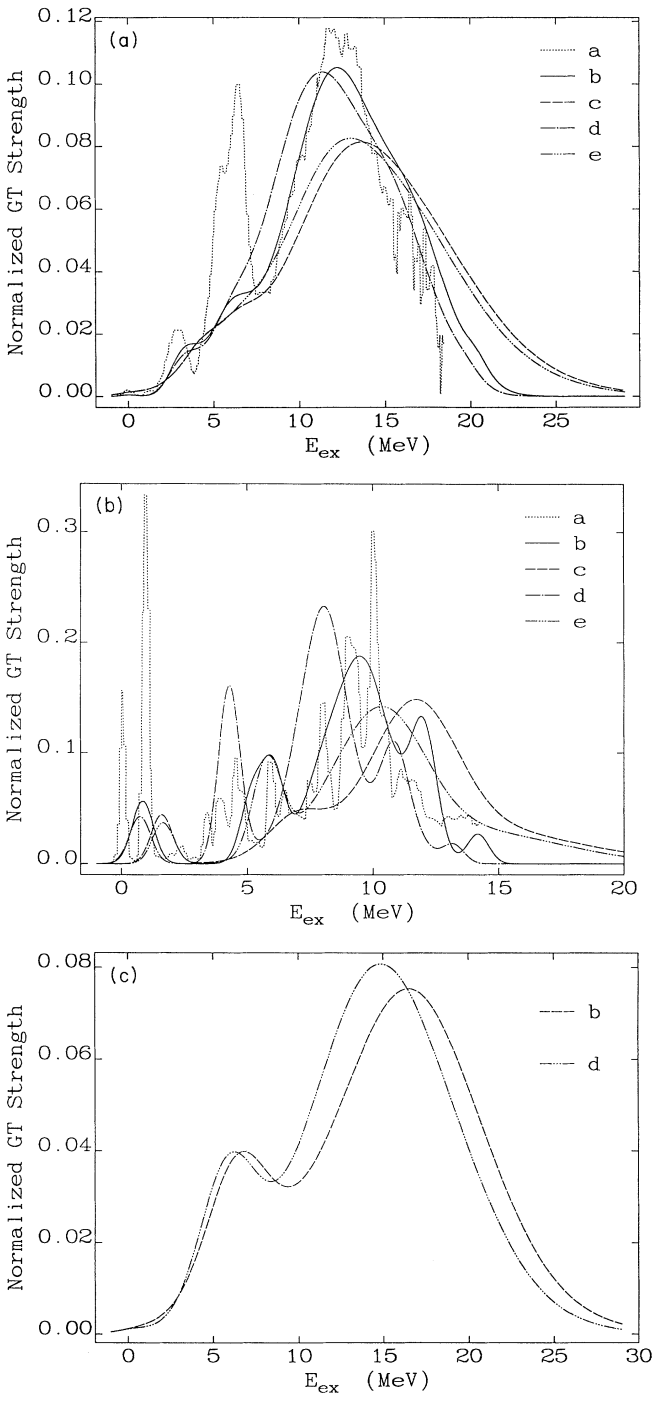

FIG. 3. Comparison of the measured cross section in the (p,n) direction with shell-model calculations for (a) ^{51}V, (b) ^{54}Fe, and (c) ^{59}Co. In each case, curve a is the experimentally measured strength function, curve b (c) is the GT strength function obtained using the small (large) model space, and curve d (e) is the GT strength function obtained using the small (large) model space with single-particle energies which optimize the fit to the measured (n,p) strength function. All curves have been normalized for comparison. For ^{59}Co, curve a is missing because there are no experimental data for this reaction. Curves c and e are missing because the model space is too large to calculate.

TABLE II. The top three rows of the table refer to calculations of S_-, while the bottom three rows refer to calculations of S_+. The number of particles for each model space is the number of nucleons in the $1p0f$ shell. The first entry for each nucleus is the small model space and the second is the large model space. When, as in the case of the small ^{51}Cr model space, more than one configuration is listed, the model space consists of a sum of all listed configurations.

Nucleus	Parent Model space	Dim.	Nucleus	Daughter Model space	Dim.
^{51}V	$(0f_{7/2})^{11}$	6	^{51}Cr	$(0f_{7/2})^{11,10}(1p_{3/2}1p_{1/2}0f_{5/2})^{0,1}$	2 421
	$(0f_{7/2})^{11,10}(1p_{3/2}1p_{1/2}0f_{5/2})^{0,1}$	522		$(0f_{7/2})^{11,10,9}(1p_{3/2}1p_{1/2}0f_{5/2})^{0,1,2}$	40 918
^{54}Fe	$(0f_{7/2})^{14}$	4	^{54}Co	$(0f_{7/2})^{14,13}(1p_{3/2}1p_{1/2}0f_{5/2})^{0,1}$	516
	$(0f_{7/2})^{14,13}(1p_{3/2}1p_{1/2}0f_{5/2})^{0,1}$	328		$(0f_{7/2})^{14,13,12}(1p_{3/2}1p_{1/2}0f_{5/2})^{0,1,2}$	14 960
^{59}Co	$(0f_{7/2})^{15}(1p_{3/2}1p_{1/2}0f_{5/2})^{4}$	447	^{59}Ni	$(0f_{7/2})^{16,15,14}(1p_{3/2}1p_{1/2}0f_{5/2})^{3,4,5}$	76 907
	$(0f_{7/2})^{15,14}(1p_{3/2}1p_{1/2}0f_{5/2})^{4,5}$	20 858		$(0f_{7/2})^{16,15,14,13}(1p_{3/2}1p_{1/2}0f_{5/2})^{3,4,5,6}$	1072 467
^{51}V	$(0f_{7/2})^{11}$	6	^{51}Ti	$(0f_{7/2})^{10}(1p_{3/2}1p_{1/2}0f_{5/2})^{1}$	38
	$(0f_{7/2})^{11,10}(1p_{3/2}1p_{1/2}0f_{5/2})^{0,1}$	522		$(0f_{7/2})^{10,9}(1p_{3/2}1p_{1/2}0f_{5/2})^{1,2}$	1 513
^{54}Fe	$(0f_{7/2})^{14}$	4	^{54}Mn	$(0f_{7/2})^{13}(1p_{3/2}1p_{1/2}0f_{5/2})^{1}$	70
	$(0f_{7/2})^{14,13}(1p_{3/2}1p_{1/2}0f_{5/2})^{0,1}$	328		$(0f_{7/2})^{13,12}(1p_{3/2}1p_{1/2}0f_{5/2})^{1,2}$	3 592
^{59}Co	$(0f_{7/2})^{15}(1p_{3/2}1p_{1/2}0f_{5/2})^{4}$	447	^{59}Fe	$(0f_{7/2})^{15,14}(1p_{3/2}1p_{1/2}0f_{5/2})^{4,5}$	2 170
	$(0f_{7/2})^{15,14}(1p_{3/2}1p_{1/2}0f_{5/2})^{4,5}$	20 858		$(0f_{7/2})^{15,14,13}(1p_{3/2}1p_{1/2}0f_{5/2})^{4,5,6}$	66 425

quasieigenstate has been added in quadrature to an experimental width of 1 MeV, in order to provide the appropriate experimental "smearing." Figures 3(a)–3(c) and 4(a)–(4c) show the results of our shell-model calculations of S_- and S_+ for ^{51}V, ^{54}Fe, and ^{59}Co, and will be discussed below. For each figure, curve *a* shows the experimental measurement. Curve *b* (*c*) shows the small (large) model space results, with no shifting of single particle energies. Curve *d* (*e*) shows the small (large) model space results, with shifting of single-particle energies which will be described below.

Figure 3(a) shows the GT strength function for ^{51}V in the (p,n) direction in greater detail. These data are compared with our shell-model calculations. The small model space strength function reproduces the experimental strength function quite well. The giant resonance and the peaks seen at ~ 3 and ~ 6 MeV are reproduced. Because of the presence of the IAS at 6.61 MeV, it is difficult to know how much of the experimentally observed strength in this region is actually GT. It should be noted that there has been no adjustment of single-particle energies to fit the giant resonance.

The larger model space does not provide as good agreement. All of the features of the strength function are shifted slightly higher in energy. The giant resonance has shifted ~ 1.5 MeV upwards. It appears that the extra nucleon in the $(2p_{3/2}2p_{1/2}1f_{5/2})$ manifold tends to block GT transitions, pushing the strength higher in energy. This trend is also seen in Table III, which lists the total strength seen in each calculation. As we go to a larger model space, the amount of GT strength diminishes. This behavior is consistent with the blocking of GT transitions in the larger model space. Curves *d* and *e* will be discussed below.

Figure 3(b) compares the measured GT strength function for ^{54}Fe with the shell-model calculations done here. Again, the small model space does a good job of fitting the giant resonance and a moderately good job of fitting the strength at lower energies (as before, none of the single-particle energies have been adjusted). The peak observed at 0.937 MeV is reproduced with 61% of the strength observed (after the overall quenching factor of 0.46 has been applied to the shell model strength function) and it is only 0.1 MeV from the correct location in energy. The structure seen near 5 MeV in the (p,n) reaction is not reproduced as well, but the shell model does predict a sizeable amount of strength in the vicinity of 6 MeV. An interesting feature in the calculation is a satellite peak located at 12 MeV. The measurement also hints at a peak in this region, but with much weaker strength. Because of the background contributions from higher multipoles at such high energies, it is possible that the experiment may have been insensitive to GT strength in this region.

As with ^{51}V, using the large model space for ^{54}Fe gives a poorer fit to the measured giant resonance. The strength function calculated using the larger model space is shifted upward by roughly 2.3 MeV relative to that of the small space. The lowest peak has been shifted upward by 0.8 MeV and its strength is 48% of the observed strength (where the shell-model strength has again been quenched). The strength near 5 MeV in the experiment has been shifted upward to roughly 7.1 MeV. The general behavior of the larger model space is consistent with what was seen in ^{51}V. It is likely that the same explanation applies. Table III shows the same reduction of strength with increasing model space size. Curves *d* and *e* will also be discussed below.

Figure 3(c) shows the calculated GT strength of ^{59}Co in the (p,n) direction. The strength has never been measured, and it was only possible to compute the strength function for the small space. It is reasonable to expect that the shell model will be trustworthy in this case, as it has been for ^{51}V and ^{54}Fe. The strength function exhibits the same general morphology as ^{51}V and ^{54}Fe, i.e., a giant resonance at high energies, and a smaller peak at inter-

TABLE III. For each nucleus, the first (second) row lists GT strength and quenching factors for the small (large) model space, and the values in the third (fourth) row are derived from the small (large) model space with shifted single particle energies. Column 4 lists the total strength estimated with the FFN methods. $\mathcal{Q}_{-,+}$ lists the quenching in the (p,n) and (n,p) channels, respectively. $^{\dagger}S_-$ for both model spaces in ^{59}Co has been determined by using the sum rule.

Nucleus	$B(\mathrm{GT})_-$	$B(\mathrm{GT})_+$	$B(\mathrm{GT})_+$(FFN)	$\mathcal{Q}_-$	$\mathcal{Q}_+$
^{51}V	20.14	5.14	5.14	0.63±0.13	0.29±0.01
	18.94	3.94		0.67±0.13	0.38±0.01
	20.14	5.14		0.63±0.13	0.29±0.01
	18.88	3.88		0.67±0.13	0.38±0.01
^{54}Fe	16.29	10.29	10.29	0.46±0.04	0.30±0.06
	15.31	9.31		0.49±0.05	0.33±0.06
	16.29	10.29		0.46±0.04	0.30±0.06
	15.22	9.22		0.49±0.05	0.34±0.06
^{59}Co	23.22	8.22	12.00		0.29±0.01
	21.68†	6.68			0.36±0.01
	21.98	6.98			0.34±0.01
	21.00†	6.00			0.40±0.01

mediate energies. However, in this nucleus, the overall scale is larger than in the previous nuclei. The giant resonance is centered near 16.4 MeV and the intermediate peak is centered at 6.7 MeV. It appears that the larger number of nucleons in the $(2p_{3/2}2p_{1/2}1f_{5/2})$ manifold has pushed the resonances to much higher excitation energies in the daughter nucleus. Table III indicates that ^{59}Co has much greater strength in the (p,n) direction than either ^{51}V or ^{54}Fe. The extra neutrons evidently provide the additional strength.

Figure 4(a) compares the GT strength of ^{51}V measured in the (n,p) direction with the shell-model calculations. The agreement is not as good as in the (p,n) channel. The small model space places most of the strength at 5.9 MeV, 0.9 MeV above the location of the measured strength. Proceeding to a larger model space improves the fit by broadening the distribution of strength.

Figure 4(b) compares the (n,p) GT strength for ^{54}Fe with the shell-model calculations. In this case, the measured strength is lower in daughter excitation energy than the results of either of the model spaces. The small model space places the strength in peaks at 3.3 and 5.9 MeV. Increasing the size of the model space introduces a spreading of the strength, but there is little improvement in the location of the strength, which migrates upward of 0.3 MeV in the larger space.

Figure 4(c) plots the measured and calculated GT strength functions for ^{59}Co in the (n,p) directions. Again the shell-model calculations place the strength at higher energies than seen experimentally. Both model spaces place the GT peak roughly 0.75 MeV higher in the daughter nucleus than was seen experimentally. The larger model space broadens the strength and thus more strength extends to higher energies.

It is possible to obtain better fits to the measured (n,p) strength functions if the single-particle energies are shifted. Curves *d* and *e* in Figs. 4(a), 4(b), and 4(c) demonstrate the results of such shifts. Table IV demonstrates how the single-particle energies had to be shifted so as to fit S_+ in each nucleus. The small model space with modified single-particle energies reproduces the centroid of each strength function (as it was designed to do), but the calculated distribution for ^{51}V and ^{54}Fe also exhibit peaks which are not seen experimentally. The calculation for ^{51}V exhibits too much strength at 2.8 MeV, while the

TABLE IV. Single-particle energies used in the calculations. Energies are given in MeV. The last two columns list the shifted single particle energies from the fit to S_+ for the nuclei. Only the $1f_{5/2}$ single-particle energies have been shifted. For the $1f_{5/2}$ energies, the first (second) row shows the shifts required for the small (large) model spaces.

Orbital	Original	^{54}Fe	^{51}V, ^{59}Co
$2p_{1/2}$	−2.474	−2.474	−2.474
$2p_{3/2}$	−5.353	−5.353	−5.353
$1f_{5/2}$	−0.263	−1.763	−1.263
		−2.263	−1.013
$1f_{7/2}$	−7.163	−7.163	−7.163

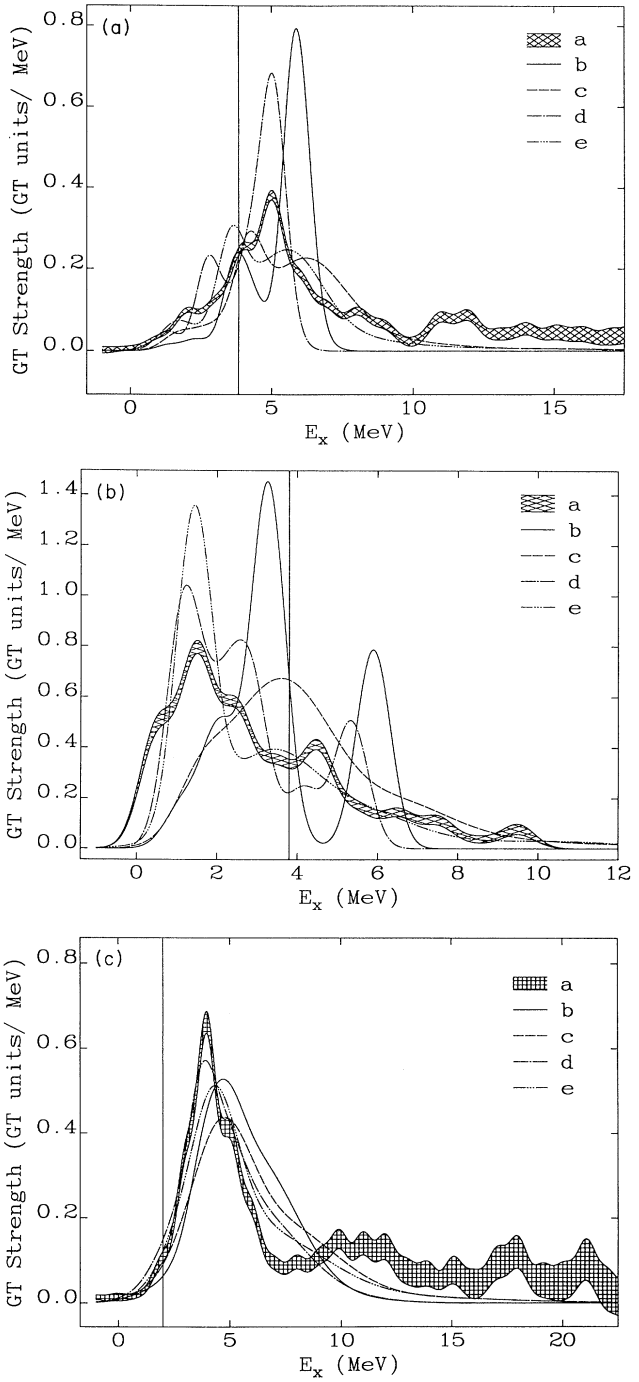

FIG. 4. Comparison of the measured GT strength function in the (n,p) direction with shell-model calculations for (a) ^{51}V, (b) ^{54}Fe, and (c) ^{59}Co. In each case, curve *a* is the experimentally measured strength function, curve *b* (*c*) is the GT strength function obtained using the small (large) model space, and curve *d* (*e*) is the GT strength function obtained using the small (large) model space with single-particle energies which optimize the fit to the measured (n,p) strength function. The solid vertical line in each case shows where the FFN method would place the GT resonance for each nucleus. Each shell-model strength function has been quenched by the overall factor $\mathcal{Q}_+$ given in Table III, in order to make comparison easier.

^{54}Fe calculation exhibits an unphysical peak at 5.3 MeV. Another deficiency of the small shifted model spaces is their tendency to concentrate the space too tightly. This is a relic of the small model spaces used. The large model space with modified single-particle energies is more successful at reproducing the measured strength functions. The strength tends to be more broadly distributed, in better agreement with the experiments. However, all of the calculations predict a too rapid decrease in strength at low energies in ^{54}Fe$(n,p)^{54}$Mn.

Curves *d* and *e* in Figs. 3(a), 3(b), and 3(c) show what happens to S_- when these shifts are used. The strength in the small shifted model space tends to be too low in the daughter spectrum by roughly 2 MeV. However, the strength for the large shifted model space is in fairly good agreement with the experiments. The strength is slightly high in the daughter, but in much better agreement than the large, unshifted model space. Thus, for the large, shifted space, the agreement between calculation and experiment is good in both the (p,n) and the (n,p) channels. None of the other model spaces exhibit good agreement for both channels.

Table III also lists the quenching in S_- and S_+, denoted by $\mathcal{Q}_-$ and $\mathcal{Q}_+$, respectively. These quenching factors are defined similarly to Eq. (2):

$$\mathcal{Q}_\pm = \frac{S_\pm(\text{Expt.})}{S_\pm(\text{Theory})} \ . \tag{3}$$

The quenching in the (n,p) direction, $\mathcal{Q}_+$, ranges from 0.29 to 0.40, with the small (large) model spaces having an average quenching factor of 0.30 (0.37). The quenching in the (p,n) direction, $\mathcal{Q}_-$, is ~ 0.65 for ^{51}V, but ~ 0.48 for ^{54}Fe. It thus appears that $\mathcal{Q}_+$ is essentially the same for all nuclei. If one assumes that $\mathcal{Q}_+$ and $\mathcal{Q}_{\rm SR}$ [as defined in Eq. (2)] are general features of *fp* shell nuclei, it is possible to use theoretical calculations to predict the actual amount of strength measured in both channels. This approach was used in the previous section, to predict the $B(\text{GT})_- = 13.5$ for ^{59}Co. If this prediction is correct, $\mathcal{Q}_-$ for ^{59}Co would be 0.61, somewhat less than the case of ^{51}V because of the larger theoretical strength in the (p,n) channel for ^{59}Co.

It is interesting to compare these results with what the Fuller, Fowler, and Newman approach [9] (hereafter FFN) would predict about S_- for these three nuclei. In this approach, the GT resonant transition for ^{51}V, ^{54}Fe, and ^{59}Co is dominated by the conversion of a $1f_{7/2}$ proton to a $1f_{5/2}$ neutron. Such a conversion results in an excited state of the daughter nucleus. The energy of the GT resonance (GTR) above the daughter ground state, E(GTR), is estimated in the FFN method by

$$E(\text{GTR}) = (\epsilon_{1f5/2} - \epsilon_{2p3/2})_n + \Delta E_{\rm ph} \tag{4}$$

for ^{51}V and ^{54}Fe, where the ϵ's are neutron single-particle energies and $\Delta E_{\rm ph}$ is the particle-hole repulsion which must be paid in elevating the neutron from its ground state to the GT resonance state (taken by FFN to be 2.0 MeV). For ^{59}Co, E(GTR) becomes

$$E(\text{GTR}) = (\epsilon_{1f5/2} - \epsilon_{1ft/2})_n + \Delta E_{\rm ph} \ . \tag{5}$$

For the single-particle energies which FFN used

$$(\epsilon_{1f52} - \epsilon_{2p3/2})_n = 6.8 \text{ MeV}/A^{1/3} \ ,$$

thus E(GTR) is 3.83, 3.80, and 2.0 MeV for ^{51}V, ^{54}Fe, and ^{59}Co, respectively. The solid vertical lines on Figs. 4(a)–4(c) show these locations for comparison with the full shell-model calculations and the experiments. It can be seen in each case that the full shell-model results are closer to the S_- actually observed.

The FFN approach also provides a method of estimating $B(\text{GT})_+$. The total strength for these nuclei is estimated by

$$B(\text{GT})+(\text{FFN}) = \frac{n_p^i n_h^f}{2j_f+1} |M_{\rm GT}^{sp}|_{if}^2 \ , \tag{6}$$

where, in these cases, n_p^i is the number of protons in the $1f_{7/2}$ orbital in the parent nucleus, n_h^f is the number of holes in the $1f_{5/2}$ neutron orbital in the parent, j_f is $\frac{5}{2}$, and $|M_{\rm GT}^{sp}|_{if}^2$ is the matrix element for single-particle transitions from the $1f_{7/2}$ orbital to the $1f_{5/2}$, as defined by FFN. For each nucleus the strength is given by

$$^{51}\text{V:} \quad B(\text{GT})_+(\text{FFN}) = \frac{3\times 6}{6}\frac{12}{7} \ , \tag{7}$$

$$^{54}\text{Fe:} \quad B(\text{GT})_+(\text{FFN}) = \frac{6\times 6}{6}\frac{12}{7} \ , \tag{8}$$

$$^{5}\text{Co} \quad B(\text{GT})_+(\text{FFN}) = \frac{7\times 6}{6}\frac{12}{7} \ . \tag{9}$$

These strengths are listed in Table III for comparison with the full shell-model results. The small model space calculations for ^{51}V and ^{54}Fe agree with the FFN results, because of the simplicity of the small model space. The FFN method predicts much more strength for ^{59}Co than does the full shell model. The FFN method is not able to include the effects of neutron blocking, which the full shell model is successful in modelling, which results in the differences seen in ^{59}Co. FFN would quench this strength by a factor of 2 and place all of it at E(GTR). As can be seen in Table III, this results in too much strength appearing at excitation energies which are too low.

In Table IV, the shifts in single-particle energies required to fit S_+ are listed. It can be seen that, for each model space, the $1f_{5/2}$ shifts are the same for ^{51}V and ^{59}Co, but different for ^{54}Fe. In Fig. 5, we have plotted these $1f_{5/2}$ single-particle energies as a function of $N-Z$, the difference between number of neutrons and protons in each nucleus. For ^{54}Fe, $N-Z=2$, while for ^{51}V and ^{59}Co, $N-Z=5$. It appears that, given the $N-Z$ of the parent nucleus, it is possible to choose the optimal shifting of single particle energies, using the following linear relationships:

$$\epsilon_{1f5/2} = -2.0963 + 0.1667(N-Z) \quad \text{small space} \ , \tag{10}$$

$$\epsilon_{1f5/2} = -3.0963 + 0.4167(N-Z) \quad \text{large space} \ . \tag{11}$$

These are the curves plotted in Fig. 5.

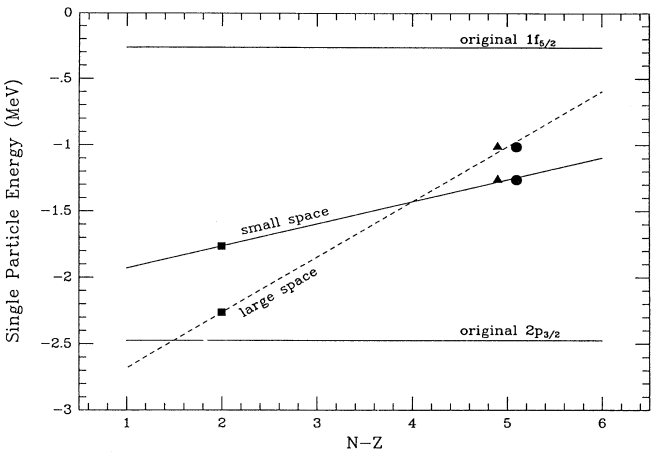

FIG. 5. Dependence of single-particle energy shifts on neutron excess. The squares refer to the shifted values of the $1f_{5/2}$ single-particle energy for ^{54}Fe. The triangles (circles) refer to the shifted values of the $1f_{5/2}$ single-particle energy for ^{51}V (^{59}Co). The lines are the fits given in Eqs. (10) and (11).

IV. CONCLUSIONS

Figures 3(a)–3(c) and 4(a)–4(c) demonstrate that shell-model calculations using an interaction calibrated by low-energy properties of *fp* shell nuclei are not successful at reproducing the strength observed in the (n,p) channel, but are fairly successful at reproducing the (p,n) strength. The best fits to experiment were obtained by using the large model space with a shifted single-particle energy. It is not surprising that such calibrations are necessary since these GT resonances are collective excitations, which are not reflected very well by low-energy properties of these nuclei. It is likely that any effective interaction for the *fp* shell would require similar shifts.

Comparison between the experiments and calculations also indicates some interesting properties of the quenching of $B(\mathrm{GT})_-$, $B(\mathrm{GT})_+$, and the sum rule. Table I indicated that the total quenching of the sum rule has a value of $\mathcal{Q}_{\mathrm{SR}}=0.74$ for both ^{51}V and ^{54}Fe. This value is consistent with $\mathcal{Q}_{\mathrm{SR}}=0.71\pm^{0.08}_{0.15}$, reported for ^{48}Ca by Rapaport *et al.* [16]. It thus appears that the quenching of the sum rule in the *fp* shell has a value of ~ 0.74. The quenching of strength in the (n,p) channel also exhibits a similar uniformity of $\mathcal{Q}_+ \approx 0.33$. This value for $\mathcal{Q}_+$ is consistent with the estimate of 0.37 made by Toki and Castel [24] for ^{54}Fe using the Tamm-Dancoff approximation. It is not clear why amount of quenching in the (n,p) channel should be a general feature of *fp* shell nuclei. Because the sum rule must be satisfied in calculations, the amount of quenching in the (p,n) channel varies among the nuclei. For ^{51}V, ^{54}Fe, and ^{59}Co, we obtained $\mathcal{Q}_- \approx 0.65$, 0.48, and 0.61, respectively.

Besides the light which has been shed on quenching in the *fp* shell, this work has important consequences for weak-interaction rates which become important during the formation and collapse of the iron core. As was discussed in the Introduction, stellar electron-capture rates are very sensitive to S_+. It has been found that shell-model calculations must use shifted single-particle energies in order to accurately locate the GT resonance in the daughter nucleus. The FFN estimates were seen to be less accurate than the original shell-model calculations. The effects of these inaccuracies can be dramatic. It has been found that, for ^{59}Co and ^{60}Co, the electron-capture rates using calibrated shell-model calculations are factors of 10–30 times weaker than the FFN rates, simply because of the placement of resonances [13]. FFN placed the resonance too low in the daughter nucleus, thus unphysically enhancing the electron-capture rate. The case of ^{54}Fe demonstrates that there may be cases in which the FFN rates are too weak, since here FFN place the resonance at too high an energy in the daughter nucleus. Detailed calculations of many nuclei will be necessary to resolve this problem.

Although the location of the GT resonance is important, the amount of quenching in each direction is also important, since calculation of electron-capture rates requires the absolute amount of strength in each direction. The apparent uniformity of $\mathcal{Q}_{\mathrm{SR}}$ and $\mathcal{Q}_+$ is extremely useful in this regard. Using the sum rule and a theoretical calculation of either $B(\mathrm{GT})_-$ or $B(\mathrm{GT})_+$ one can compute the actual amount of strength in both channels. It is now possible to calculate electron capture and beta decay rates for nuclei in the *fp* shell much more accurately than has been done in the past.

ACKNOWLEDGMENTS

We thank the CHARGEX group at TRIUMF for making its data available before formal publication and Dr. W. P. Alford for useful discussions on how to interpret these experiments. This work was performed at Lawrence Livermore National Laboratory under the auspices of the U.S. Department of Energy under Contract No. W-7405-ENG-48 and DOE Nuclear Theory Grant No. SF-ENG-48.

[1] C. D. Goodman *et al.*, Phys. Rev. Lett. **44**, 1755 (1980).
[2] T. N. Taddeucci *et al.*, Nucl. Phys. **A469**, 125 (1987).
[3] A. García *et al.*, Phys. Rev. Lett. **67**, 3654 (1991).
[4] E. G. Adelberger, A. García, and D. P. Wells, Phys. Rev. Lett. **67**, 3658 (1991).
[5] D. P. Wells, Bull. Am. Phys. Soc. **67**, 1296 (1992).
[6] M. B. Aufderheide, S. D. Bloom, D. A. Resler, and C. D. Goodman, Phys. Rev. C **46**, 2251 (1992).
[7] H. A. Bethe, G. E. Brown, J. Applegate, and J. Lattimer, Nucl. Phys. **A234**, 487 (1979).
[8] G. M. Fuller, W. A. Fowler, and M. J. Newman, Astrophys. J. Suppl. **42**, 447 (1980).
[9] G. M. Fuller, W. A. Fowler, and M. J. Newman, Astrophys. J. **252**, 715 (1982).
[10] G. M. Fuller, W. A. Fowler, and M. J. Newman, Astrophys. J. Suppl. **48**, 279 (1982).

[11] G. M. Fuller, W. A. Fowler, and M. J. Newman, Astrophys. J. **293**, 1 (1985).
[12] G. M. Fuller and B. S. Meyer, Astrophys. J. **376**, 701 (1991).
[13] M. B. Aufderheide, S. D. Bloom, D. A. Resler, and G. J. Mathews, Phys. Rev. C **47**, 2961 (1993).
[14] C. Gaarde, J. S. Larson, and J. Rapaport, in *Spin Excitations in Nuclei,* edited by F. Petrovich *et al.* (Plenum, New York, 1982), p. 65.
[15] C. D. Goodmann and S. D. Bloom, in *Spin Excitations in Nuclei,* edited by F. Petrovich *et al.* (Plenum, New York, 1982), p. 143.
[16] J. Rapaport *et al.*, Nucl. Phys. **A427**, 332 (1984).
[17] B. D. Anderson *et al.*, Phys. Rev. C **41**, 1474 (1990).
[18] M. C. Vetterli *et al.*, Phys. Rev. C **40**, 559 (1989).
[19] W. P. Alford *et al.*, submitted to Phys. Rev. C.
[20] C. D. Goodman, J. Rapaport, and S. D. Bloom, Phys. Rev. C **42**, 1150 (1990).
[21] A. van Hees and P. Glaudemans, Z. Phys. A **303**, 267 (1981).
[22] J. van Hienen, W. Chung, and B. H. Wildenthal, Z. Phys. A **269**, 159 (1976).
[23] D. A. Resler and S. M. Grimes, Comput. Phys. **2**, 65 (1988).
[24] H. Toki and B. Castel, Phys. Lett. B **219**, 181 (1989).